https://doi.org/10.1016/j.scriptamat.2022.115224

A novel maraging stainless steel ultra-high-strengthened by multi-nanoprecipitations

Jianquan Wan [a*], Haihui Ruan[b], Zhiyi Ding [c], Ling Bing Kong [a*]

[a] College of New Materials and New Energies, Shenzhen Technology University, Shenzhen, 518118, China

[b] Department of Mechanical Engineering, The Hong Kong Polytechnic University, Hung Hom, Kowloon, Hong Kong, China

[c] Department of Materials and Chemistry, University of Shanghai for Science and Technology, Shanghai, 200093, China

Abstract:

A novel ultra-high strength maraging stainless steel with a chemical composition of Fe-11.5Cr-8.5Co-8.0Ni-5.0Mo-1.2Al-0.01C (in wt.%) has been developed. It utilizes a unique combination of nanometer scale intermetallic precipitates of Laves, β-NiAl, and sigma phases to achieve an ultra-high ultimate tensile strength up to 3.15 GPa, together with balanced ductility and uniform elongation of about 2.74% and 2.05%, respectively. Maximizing the austenite content in the as-hot-rolled steel before cold-rolling and ageing treatments is essential to remove work-hardening behavior and obtain an ultra-high strength without uniform elongation loss of the maraging steel. It is found that precipitation hardening sharply peaks at the ageing temperature of 525 °C for 3.5 h, which is mainly due to the peak strengthening effect of net-like sigma phase through its transcrystalline fracture, which forms small globular particles during tensile deformation.

Key words: Ultra-high strength; Maraging steel; Deformation-induced martensite transformation; Nanoprecipitation

* Corresponding author:

E-mail address: wanjianquan2013@163.com (Jianquan Wan); konglingbing@sztu.edu.cn (L. B. Kong)

Maraging steel is recognized as the king of high strength steel with acceptable ductility [1], which is continually sought after in engineering applications to service for sustainable economy. It is strengthened by both martensite and precipitation hardening, and nano-sized precipitation is designed to obtain the ultrahigh strength [2]. Since the concept of maraging steel was firstly proposed from 1960s [3], various maraging steels have been developed, such as 18Ni (250), 18Ni (300), 18Ni (350), and 13Ni (400), etc. The 18Ni (350) steel exhibits the ultimate tensile strength (UTS) and ductility of about 2.4 GPa and 8.9%, respectively [4]. By increasing the contents of Co and Mo, the 13Ni (400) steel was designed to obtain an UTS of 2.8 GPa, but it is difficult to be realized in most cases [5]. Various precipitates have been found in strengthening maraging steels, depending on chemical composition and heat treatment, such as η-phase ($Ni_3(Ti, Al)$) [6], G-phase [7], and copper precipitates [8], etc. The traditional 18Ni maraging steels [9, 10] mainly utilize Ni_3Ti and Laves precipitates to realize the strengthening effect, while the present work is aimed at developing a low Ni and low Co maraging stainless steel through strengthening by three nanometre-sized intermetallic precipitates, namely β-NiAl, Laves, and sigma (σ) phases. The purposes are threefold. First, we want to decrease the particle size of precipitates by forming multiple types of precipitates, e.g., the β-NiAl particles in this work are much smaller and denser than those introduced by Suna et al. [11] in their development of a maraging steel strengthened by β-NiAl and Laves phases. Second, the co-precipitation of multiple types of nanoparticles is more attractive than the dispersion of a single type of nanoparticle because the former may lead to a better combination of mechanical properties resulting from the synergistic effect of multiple types of nanoparticles [12, 13]. Lastly, we intend to utilize peak-strengthening effect of the σ phase with a net-like shape formed during the over ageing treatment which was found in our previous study [14]. It is noted that some maraging steels contained three precipitates, e.g., Custom 455 (Copper nanoclusters, Ni_3Ti, and $Ni_3(Ti, Al)$) [15] and 13Cr-13Co-4.5Ni-3.5Mo-

0.5Ti (Mo-rich R′, Ni_3(Ti, Al), and Cr-rich α') [16], obtaining the UTS of about 2 GPa after proper ageing treatments.

Although the precipitation behavior in maraging steels has been extensively investigated, austenitizing the steels before cold-rolling and ageing treatments, which can maximize the martensite transformation and enhance the strength of maraging steel, is rarely discussed in the open literature. Herein, we specially clarify the effects of two types of ferrites called δ and α phases. The δ phase originates from non-equilibrium solidification due to an incomplete austenitic transformation, which is enriched in Cr, Mo and Al, but depleted in Ni [17]. It is extremely difficult to the dissolve δ phase in subsequent forging and thermo-mechanical treatments. Note that a long-time high-temperature diffusion process can reduce δ phase, but it causes burning loss and grain coarsening of the steel [18, 19]. The α phase originates from solid-state phase transformation which is the consequence of non-equilibrium phase transformation from γ phase during cooling of the steel. It also reduces martensitic phase and debates mechanical performances. Therefore, the development of a ultrahigh-strength maraging steel must involve the further understanding of the evolution of both ferritic phases and the co-precipitation of various nanoparticles.

The present maraging steel has a specific composition of Fe-11.5Cr-8.5Co-8.0Ni-5.0Mo-1.2Al-0.01C (in wt.%) obtained by spectroscopic analysis. In maraging steels, additions of Co and Ni promote the formation of Mo-enriched [20] and NiAl precipitates [11], respectively. The casting was hot-rolled at 1250 °C for 2 h, leading to steel sheets with 6 mm thickness. Specimens with gage length of 10 mm were used for tensile test at room temperature, with the initial strain rate of 10^{-3} s^{-1}. The thickness of tensile samples were measured by height indicator at the left, middle, and right sides of the gage part, and their average value is taken as final one. Vickers indentations were performed with a load of 50

mN during 10 s using FM-ARS9000, FUTURE-TECH JAPAN. For each sample, a minimum of 10 indentations were performed. The fracture surface of tensile samples were examined by using a field-emission scanning electron microscope (SEM, Zeiss Merlin) equipped with an energy dispersive X-ray spectrometry (EDS). The detailed design of transmission electron microscope (TEM), atom-probe tomography (APT), and corrosion property experiments were shown in **Supplementary Text.** All the solution treatments were conducted with water quenching after heating. Cold rolling (CR) with 65% and 90% thickness reductions were conducted along the hot rolling direction of samples, and steel sheets with thickness of about 2.1 and 0.6 mm were obtained, respectively. It was found that martensite was reversed to γ phase at ageing temperatures of about 650 °C and above as indicated in **Fig. S1**. Thus, no reverted γ phase was formed in the CR steel samples after ageing at 525 °C. The XRD analysis was performed using a Cu-Kα radiation for phase identification, and volume fraction of the γ phase is calculated based on the integrated intensities of diffraction peaks pertaining to δ (200), δ (211), γ (200), γ (220), and γ (311) [21]. Volume fraction of the γ phase can be calculated by using the following formula [22, 23]:

$$f_r = \frac{\frac{1}{n}\sum_{j=1}^{n}\frac{I_r^j}{R_r^j}}{\frac{1}{n}\sum_{j=1}^{n}\frac{I_r^j}{R_r^j}+\frac{1}{n}\sum_{j=1}^{n}\frac{I_\delta^j}{R_\delta^j}} \quad (1)$$

where R is the theoretical intensity for a crystallographic plane and given in Ref. [23], I is the integrated intensity for the plane, and n is the number of diffraction peaks examined.

According to the XRD pattern shown in Fig. 1(a), the as-hot-rolled steel contained about 70 vol.% γ phase and 30 vol.% ferrite or α'-martensite phase, since ferrite and α'-martensite phases exhibit the same peaks. TEM test was used to study the microstructural features as shown in Fig. 1(b), and the corresponding selected area diffraction pattern (SADP) in the

inset confirmed that it is the ferrite instead of α'-martensite phase. About 6 vol.% and zero contents of γ phase were remained in 65% and 90% CR samples, respectively, as indicated by another two XRD patterns shown in Fig. 1(a). Therefore, it can be concluded that large plastic deformation promotes the α' martensite formation in the maraging steel [24]. The 65% and 90% CR samples were conducted with ageing at 525 °C for 2 h, and they are denoted as 65CRA and 90CRA, respectively. The Vickers hardness of these samples as a function of cold rolling ratio and ageing were shown in Fig. 1(c). Micro-hardness values are about 200, 380, and 400 HV for as-hot-rolled, 65% and 90% CR samples, respectively. They are further increased to 507 and 663 HV for 65CRA and 90CRA samples, respectively. It suggests that both plastic deformation and ageing exhibit a significant hardening effect for steels, and the latter is apparently stronger than the former, which is the rationality of developing nano-precipitation strengthening [25]. Tensile stress-strain curves of 65CRA and 90CRA samples are shown in Fig. 1(d). The 65CRA sample exhibits UTS and ductility of about 2.24 GPa and 5.2%, respectively. Comparatively, UTS and ductility of the 90CRA sample are increased and decreased by 18.3% and 28.8%, with corresponding values of 2.65 GPa and 3.7%, respectively. It suggests that increase of the CR ratio followed with ageing leads to a significant enhancement in strength of the maraging steel. This is consistent with the finding [26] that the higher volume-fraction of α'-martensite contributes to higher flow stress of the steel. It is well known that the sub-microstructure of α′ martensite is characterized by high density dislocations, so the increased α' martensite content promotes the strength of a steel due to the enhancement in the dislocation strengthening effect [27]. The TEM image in Fig. 1(e) shows that the average width of martensite laths in the 90CRA sample is only about 47.4 nm, which is responsible for ultra-high strength of the steel matrix, according to the Hall-Petch relationship [28]. More severe plastic deformation not only promotes the formation of α′ martensite which provides a proper matrix for age hardening but also induces more

dislocations which provide additional nucleation sites for the formation of precipitates during ageing [29]. Therefore, the 90CRA steel is an ideal candidate to achieve an ultra-high strength maraging steel through proper thermo-mechanical treatments [30].

Tensile curve of the 90CRA sample exhibits a work-hardening exponent of about 0.15, as calculated by the Ludwik equation [31]:

$$\sigma_T = \sigma_y + k\varepsilon^n \quad (2)$$

where n, σ_T, ε, σ_y, and k are work-hardening exponent, true stress, true strain, yield strength (YS), and strength coefficient, respectively. It is significantly different with tensile curves of typical maraging steels [32, 33] which have no any work-hardening behavior. It should be attributed to the ferrite phase in the as-hot-rolled sample which is remained in the steel after cold rolling and ageing treatments. Thus, a proper heat treatment was applied to as-hot-rolled steel samples to maximize the γ phase content, because plastic deformation can not be applied since it changes the microstructure of γ phase. Volume fractions of the γ phase versus annealing temperature and time are shown in Fig. 2 (a, b). The γ phase content is maximized at annealing temperature of 600 °C as shown in Fig. 2(a), while annealing time also affects stability of the metastable γ phase as observed in Fig. 2(b). The γ phase content is maximized at 89 vol.% due to the undissolved δ phase, when the as-hot-rolled steel was solution-treated at 600 °C for 1 h. Thus, the as-hot-rolled sample was solution-treated at 600 °C for 1 h followed with 90CR and then ageing at 525 °C for 2 h, and it is denoted as 600-90CRA. Its tensile curve is shown in Fig. 2(c). Compared to the 90CRA sample, UTS and ductility of the 600-90CRA sample are increased and decreased by 7.5% and 21.6%, with corresponding values of 2.85 GPa and 2.9%, respectively. However, they are about the same uniform elongation of 2.8%, which is the strain that true stress and work hardening rate are coincident at the maximum load point. Also, the tensile curve of 600-90CRA sample shows no work-

145 hardening behavior as that of typical maraging steels.

146 APT investigation was applied to the 600-90CRA sample to analyze the precipitates,
147 and three precipitations were revealed. They are NiAl, Fe-Cr, and Mo-enriched phases,
148 respectively, as shown in Fig. 3(a). The NiAl phase consists of almost spherical particles with
149 an average size of several nanometers, which are distributed evenly throughout the matrix.
150 Particles of the Fe-Cr phase exhibit a similar average size as that of the NiAl phase, with
151 more irregular shapes and a lower number density. However, the Mo-enriched phase exhibits
152 an average particle size of about 20 nm, with irregular shapes and an uneven distribution [34],
153 which makes it difficult to determine its number density. The Co element shows no
154 partitioning as shown in Fig. 3(b), which is consistent with the finding that it does not form
155 precipitations during an ageing process due to the high Fe-Co binding energy [20].
156 Quantification of the solute partitioning between nanoparticles and the matrix in the 600-
157 90CRA sample was calculated from proximity histograms [35] shown in Fig. 3(c-e), in which
158 the average three-dimensional compositional information with respect to the distance from
159 the particle/matrix interface is demonstrated. Fig. 3(c) shows an apparent partitioning of Ni
160 and Al elements in the nanoparticle which contains not pure NiAl but also contains Fe.
161 Quantitative analysis shows that it is a Ni/(Al+Fe) atomic ratio of 1.14, which indicates that
162 Fe atoms occupy the sites of Al. It is a B2-type Ni (Al, Fe) nanoparticle, called β-NiAl phase.
163 Fig. 3(d) shows an apparent partitioning of Mo and Cr elements in the nanoparticle, and the
164 quantitative analysis shows that the stoichiometric composition of the nanoparticle is (Fe,
165 $Cr)_2$ Mo. It is the Laves phase [36] which tends to form at boundaries, with sizes in the range
166 of 10-several 100 nm [37]. In Fig. 3(e), the partitioning of Cr element in the nanoparticle is
167 apparent, and the corresponding stoichiometric composition is $Fe_{60}Cr_{40}$, which is known as a
168 sigma (σ) phase. Based on the well-known Orowan mechanism, the increase in the YS of a
169 steel due to precipitation strengthening is attributed to the decrease in particle size and the

increase in density of the precipitates. It increases not only the force of dislocation movement but also the dislocation density, which are particular significant to achieve ultrahigh strength of the maraging steel [38]. The average radius and number density of these nanoparticles are summarized in Table 1. Such intensive nanoprecipitations are responsible for high strength of the maraging steel [39]. Among these precipitates, the *β*-NiAl phase has a high coherency with the BCC matrix, and the coherent nanoparticles tend to nucleate uniformly in the matrix with ultra-fine particle sizes [40-42]. It exhibits a lattice mismatch with the surrounding martensitic matrix low to 0.14%. These nanoparticles keep a spherical shape when their size is below 45 nm [43], resulting in a high number density and enhanced strengthening effect [40, 44]. Since the average size of β-NiAl nanoparticle is below the critical value for Orowan looping, dislocation motion follows the particle shearing mechanism [45] in which the increase of YS results mainly from contributions of order strengthening (σ_{order}), modulus strengthening ($\sigma_{modulus}$), and coherency strengthening ($\sigma_{coherency}$). Equations for these contributions are given as follows [45]:

$$\sigma_{order} = M\left(\frac{r_{apb}^{3/2}}{b}\right)\left(\frac{4r_s f}{\pi T}\right)^{1/2} \quad (3)$$

$$\sigma_{modulus} = M\frac{Gb}{L}\left(1-\left(\frac{E_p}{E_m}\right)^2\right)^{3/4} \quad (4)$$

$$\sigma_{coherency} = 4.1MG\varepsilon^{3/2}f^{1/2}\left(\frac{R}{b}\right)^{1/2} \quad (5)$$

where all factors are detailly described in **Supplementary Text**. The strengthening contribution of β-NiAl phase is calculated and listed in Table 2, which is significantly higher than that of the NiAl precipitate [45]. It indicates that an increase in the number density of β-NiAl precipitate sharply increases the strength of a steel when it reaches nearly E24 level, in which modulus strengthening is the most significant.

The *σ* phase has a high hardness, but it is very brittle due to the topologically close-packed (TCP) structure. Thus, net-like *σ* phase particles can be refined into a stable globular

morphology through plastic deformation [46]. The impact of σ phase on the mechanical property of a steel depends on various factors, such as its volume fraction, size, morphology, and distribution in the matrix [47]. Fine and homogenous dispersion of the σ phase exhibits an enhanced precipitation-strengthening effect in a steel [46]. The σ phase is low coherent with the BCC Fe-matrix and usually precipitates in the form of coarse particles [48]. Therefore, it is sensitive to the ageing time and exhibits a strong peak-strengthening effect, especially in the Mo-added steel, which is called over ageing phenomenon [49]. The Laves phase is precipitated after the β-NiAl phase which is formed in the early stage [50]. They both exhibit a high thermodynamic stability, resulting in a stable precipitation strengthening effect upon a prolonged ageing treatment [39, 50-52]. Thus, the as-hot-rolled steel samples were solution-treated at 600 °C for 1 h followed with 90% CR and then ageing at 525 °C for 2 h~5 h, respectively. The measured micro-hardness for these ageing samples are shown in Fig. 4(a), with a peak value in the 3.5h-aged sample. A representative TEM image of the 3.5h-aged sample before tensile test is shown in Fig. 4(b). The high-angle annular dark-field (HAADF) image in Fig. 4(c) reveals that most of precipiates were evenly distributed in the martensite lath which contains numerous dislocations. The σ phase particles show a net-like structure, with an average dimension of 9.2 nm*37.5 nm (width*length). Fig. 4(d, e) display high-resolution transmission electron microscopy (HRTEM) images of Laves and β-NiAl phases, respectively, with the crystallographic information derived from the fast Fourier transform (FFT) analysis shown in their insets. It confirms the above analyses on these precipitates by APT. Finally, tensile tests were conducted on these ageing samples, and an ultra-high precipitation strengthening was observed, as shown in Fig. 5(a). For the 3.5h-aged sample, the UTS has a peak value of about 3.15 GPa, while YS, ductility, and uniform elongation are about 3.12 GPa, 2.74%, and 2.05%, respectively. Both YS and UTS decrease, while ductility increases, as the ageing time is longer than 3.5 h. HAADF image of the 3.5h-

aged sample after tensile test is depicted in Fig. 5(b). Particles of the σ phase show a spherical morphology with an average diameter of about 9.5 nm. Thus, peak strength of the 3.5h-aged sample is mainly attributed to particles of the σ phase for its transcrystalline fracture during tensile deformation. With the increasing ageing time in the range of 1.5-3.5 h, fine σ phase particles tended to aggregate and formed a net-like shape, which led to its transcrystalline fracture during tensile deformation due to the high brittle TCP structure. Thus, a large number of spherical σ particles were formed, resulting in a significant strengthening effect [49]. On the other hand, the bulky σ phase formed after ageing for longer than 3.5 h, resulting in a reduction in strength of the steel [53]. Moreover, it causes the deflection of cracks, which can even make the surrounding brittle martensite matrix fail in a ductile mode [47]. These analyses have been confirmed by the SEM test. Typical morphologies on the fracture surface of these samples aged at 525 °C for 2, 3.5, and 5 h after tensile test are shown in **Fig. S2**. The fractographic morphology of the 2h-aged sample is characterized by fine dimples, while that of the 5h-aged one exhibits large ductile dimples which is in line with the apparent necking phenomenon during the tensile test. However, on the fracture surface of 3.5h-aged sample, ultra-fine dimples are observed, which could be associated with fine intermetallic precipitates [52]. It is confirmed by the presence of σ phase particles on the fracture surface, with a chemical composition derived from EDS data and listed in Table 3. The σ phase served as the crack embryos and led to a low uniform elongation of the 3.5h-aged sample.

Through large plastic deformation combined with the co-precipitation of three nanoscale intermetallic precipitates (Laves, β-NiAl, and σ phases), a novel maraging stainless (Fig. S3) steel was developed, which has a high UTS and an acceptable uniform elongation of 2.85 GPa and 2.8%, respectively. After ageing at 525 °C for 3.5 h (peak ageing time), an ultra-high UTS of 3.15 GPa was obtained, and the uniform elongation can remain at about 2.05%.

Austenitizing the as-hot-rolled steel before cold-rolling and ageing treatments is necessary for improving its mechanical performance. It maximizes the martensite phase in the maraging stainless steel, which removes work-hardening behavior and increases strength without uniform elongation loss of the maraging steel. Large plastic deformation promotes the formation of α′ martensite transformed from the γ phase, resulting in a high-strength matrix. Furthermore, multiply types of nanoprecipitations with a high density render an even stronger strengthening effect for the maraging steel. In particular, the β-NiAl precipitate sharply increases strength of the maraging stainless steel when its density reaches E24 level, and the net-like σ phase exhibits a peak strengthening effect on the steel through transcrystalline fracturing into many small globular particles during tensile deformation.

Above results indicate that the co-precipitation through a suitable ageing treatment can bring about a maraging steel with a YS of over 3 GPa and maintain a reasonable uniform elongation of over 2%. It is noted that the δ phase is still remained in the maraging steel. If it can be totally dissolved, the maraging steel can exhibit an even better mechanical performance, and this will be our future work.

We are grateful the financial support by General Research Fund of the Hong Kong Research Grants Council (Grant No. 15213619) and the Guangdong Basic and Applied Basic Research Foundation (2020B1515120002).

Declaration of Competing Interest

The authors declare that they have no known competing financial interests or personal relationships that could have appeared to influence the work reported in this paper.

Reference

[1] C. Herrera, D. Ponge, D. Raabe, Design of a novel Mn-based 1 GPa duplex stainless TRIP steel with 60% ductility by a reduction of austenite stability, Acta Materialia 59(11) (2011) 4653-4664.

[2] S. Jiang, W. Hui, W. Yuan, X. Liu, Z. Lu, Ultrastrong steel via minimal lattice misfit and high-density nanoprecipitation, Science Foundation in China 544(02) (2017) 460.

[3] W.M.G.P. D Ultrahigh-strength steels for aerospace applications, JOM 42(5) (1990) 20-24.

[4] H.J. Rack, D. Kalish, The strength and fracture toughness of 18 Ni (350) maraging steel, Metallurgical & Materials Transactions B 2(11) (1971) 3011-3020.

[5] H. Yi, Y. Ke, W. Qu, F. Kong, G. Su, Strengthening and toughening of a 2800-MPa grade maraging steel, Materials Letters 56(5) (2002) 763-769.

[6] W. Sha, A. Cerezo, G.D.W.J.M.T.A. Smith, Phase chemistry and precipitation reactions in maraging steels: Part I. Introduction and study of Co-containing C-300 steel, 24(6) (1993) 1241-1249.

[7] A. Gemperle, J. Gemperlovã¡, W. Sha, G.D.W.J.M.S.J. Smith, Aging behaviour of cobalt free chromium containing maraging steels, 8(6) (1992) 546-554.

[8] H.R.J.M.L. Habibi, Atomic structure of the Cu precipitates in two stages hardening in Maraging steel, 59(14) (2005) 1824-1827.

[9] Chaolin, Zhou, Kesong, Wenyou, Zhang, Panpan, Kuang, Tongchun, Microstructural evolution, nanoprecipitation behavior and mechanical properties of selective laser melted high-performance grade 300 maraging steel.

[10] U.K. Viswanathan, G.K. Dey, M.K. Asundi, PRECIPITATION HARDENING IN 350-GRADE MARAGING-STEEL, Metallurgical Transactions a-Physical Metallurgy and Materials Science 24(11) (1993) 2429-2442.

[11] L. Suna, T.H. Simmb, T.L. Martinc, S. Mcadamb, D.R. Galvin, A novel ultra-high strength maraging steel with balanced ductility and creep resistance achieved by nanoscale β-NiAl and Laves phase precipitates, Acta Materialia 149 (2018) 285-301.

[12] M.D. Mulholland, D.N. Seidman, Nanoscale co-precipitation and mechanical properties of a high-strength low-carbon steel, Acta Materialia 59(5) (2011) 1881-1897.

[13] M. Kapoor, D. Isheim, S. Vaynman, M.E. Fine, Y.W. Chung, Effects of increased alloying element content on NiAl-type precipitate formation, loading rate sensitivity, and ductility of Cu- and NiAl-precipitation-strengthened ferritic steels, Acta Materialia 104 (2016) 166-171.

[14] Jianquan, Wan, Haihui, Ruan, Jianbiao, Wang, Sanqiang, S.J.M. Science, E.A.S.M.P. Misrostructure, Processing, The Kinetic diagram of sigma phase and its precipitation hardening effect on 15Cr-2Ni duplex stainless steel, (2018).

[15] T.S. Baker, Effect of Ageing Temperature on the Mechanical and Stress Corrosion Properties of Carpenter Custom 455 Stainless Steel, (1985).

[16] Yongcan, Cotton, D. James, Ryan, J. Glamm, Shen, Yifu, Wang, Shan, Yiyin, A new 1.9 GPa maraging stainless steel strengthened by multiple precipitating species.

[17] A. Rosenauer, D. Brandl, G. Ressel, S. Lukas, S. Monschein, M. Stockinger, R. Schnitzer, Influence of delta ferrite on the impact toughness of a PH 13-8 Mo maraging steel, Materials Science and Engineering a-Structural Materials Properties Microstructure and Processing 856 (2022).

[18] P. Wang, S.P. Lu, N.M. Xiao, D.Z. Li, Y.Y.J.M.S. Li, A.S.M.P. Engineering, Misrostructure, Processing, Effect of delta ferrite on impact properties of low carbon 13Cr–4Ni martensitic stainless steel, (13/14) (2010) 527.

[19] J.R. Li, J.J. Liu, B. Jiang, C.L. Zhang, Y.Z. Liu, Influence of High Temperature Pre-Deformation on the Dissolution Rate of Delta Ferrites in Martensitic Heat-Resistant Steels, Metals and Materials International 23(2) (2017) 239-245.
[20] J. Tian, M.B. Shahzad, W. Wang, L. Yin, Z. Jiang, K. Yang, Role of Co in formation of Ni-Ti clusters in maraging stainless steel, Journal of Materials Science & Technology 34(9) (2018) 1671-1675.
[21] B.B. He, H.W. Luo, M.X. Huang, Experimental investigation on a novel medium Mn steel combining transformation-induced plasticity and twinning-induced plasticity effects, International Journal of Plasticity 78 (2016) 173-186.
[22] A.K. De, D.C. Murdock, M.C. Mataya, J.G. Speer, D.K. Matlock, Quantitative measurement of deformation-induced martensite in 304 stainless steel by X-ray diffraction, Scripta Materialia 50(12) (2004) 1445-1449.
[23] Newell, H., Moser, Todd, S., Gross, Yannis, P., Korkolis, Martensite Formation in Conventional and Isothermal Tension of 304 Austenitic Stainless Steel Measured by X-ray Diffraction, Metallurgical&Materials Transactions A 45(11) (2014) 4891-4896.
[24] Y. He, K. Yang, K. Liu, W. Sha, Z.J.M. Guo, M.T. A, Age hardening and mechanical properties of a 2400 MPa grade cobalt-free maraging steel, 37(4) (2006) 1107-1116.
[25] Z. Jiao, J.H. Luan, M.K. Miller, Y.W. Chung, C.T.J.E. Liu, Co-precipitation of nanoscale particles in steels with ultra-high strength for a new era, (3) (2017).
[26] V. Seetharaman, R. Krishnan, Influence of the martensitic transformation on the deformation behaviour of an AISI 316 stainless steel at low temperatures, Journal of Materials Science 16(2) (1981) 523-530.
[27] Y.Z. Shu, E. Compagnon, B. Godin, A.M.J.M.T.P. Korsunsky, Investigation of Martensite Transformation in 316L Stainless Steel ☆, 2 (2015) S251-S260.
[28] G. Krauss, Martensite in steel: strength and structure, Materials Science and Engineering: A s 273–275(none) (1999) 40-57.
[29] X.S. Yang, S. Sun, T.Y. Zhang, The mechanism of bcc α' nucleation in single hcp ε laths in the fcc $\gamma \rightarrow$ hcp $\varepsilon \rightarrow$ bcc α' martensitic phase transformation, Acta Materialia 95 (2015) 264-273.
[30] J.R. Mihalisin, C.G. Bieber, Progress toward attaining theoretical strength with iron-nickel maraging steels, JOM 18(9) (1966) 1033-1036.
[31] Ludwik, P., Elemente der technologischen Mechanik, Springer Berlin Heidelberg 10.1007/978-3-662-40293-1 (1909).
[32] S. Yin, C. Chen, X. Yan, X. Feng, R. Jenkins, P. O'Reilly, M. Liu, H. Li, R. Lupoi, The influence of aging temperature and aging time on the mechanical and tribological properties of selective laser melted maraging 18Ni-300 steel, Additive Manufacturing 22 (2018) 592-600.
[33] P.W. Hochanadel, G.R. Edwards, C.V. Robino, M.J. Cieslak, Heat treatment of investment cast PH 13-8 Mo stainless steel: Part I. Mechanical properties and microstructure, Metallurgical and Materials Transactions A (1994).
[34] H. Cui, F. Sun, K. Chen, L. Zhang, R. Wan, A. Shan, J. Wu, Precipitation behavior of Laves phase in 10%Cr steel X12CrMoWVNbN10-1-1 during short-term creep exposure, Materials Science & Engineering A 527(29-30) (2010) 7505-7509.
[35] L.G. Sun, G. Wu, Q. Wang, J.J.M.T. Lu, Nanostructural metallic materials: Structures and mechanical properties, 38 (2020).
[36] J. Hald, Microstructure and long-term creep properties of 9–12% Cr steels, International Journal of Pressure Vessels & Piping 85(1–2) (2008) 30-37.
[37] S. Thomas, L. Sun, G. Deri, H. Paul, R. Martin, B. Soran, G. Elliot, B. Harshad, P. Karen, The Effect of a Two-Stage Heat-Treatment on the Microstructural and Mechanical Properties of a Maraging Steel, Materials 2017(10) (2017).
[38] E. Orowan, Dislocations and Mechanical Properties, (1954).
[39] H. Zhang, M. Sun, Y. Liu, D. Ma, Y. Li, Ultrafine-grained dual-phase maraging steel with high strength and excellent cryogenic toughness, Acta Materialia (2021) 116878.

[40] Z.B. Jiao, J.H. Luan, M.K. Miller, C.Y. Yu, C.T. Liu, Effects of Mn partitioning on nanoscale precipitation and mechanical properties of ferritic steels strengthened by NiAl nanoparticles, Acta Materialia 84 (2015) 283-291.
[41] W. Xu, P.E.J. Rivera-Díaz-del-Castillo, W. Yan, K. Yang, D. San Martín, L.A.I. Kestens, S. van der Zwaag, A new ultrahigh-strength stainless steel strengthened by various coexisting nanoprecipitates, Acta Materialia 58(11) (2010) 4067-4075.
[42] J. Millán, S. Sandlöbes, A. Al-Zubi, T. Hickel, P. Choi, J. Neugebauer, D. Ponge, D. Raabe, Designing Heusler nanoprecipitates by elastic misfit stabilization in Fe–Mn maraging steels, Acta Materialia 76 (2014) 94-105.
[43] R. Taillard, A. Pineau, B.J. Thomas, The precipitation of the intermetallic compound NiAl in Fe-19wt.%Cr alloys, Materials Science and Engineering 54(2) (1982) 209-219.
[44] M. Kapoor, J.-C. Wang, L. Wetherill, N. Le, S. Bertelsen, A.L. Hinrichs, J. Budde, A. Agrawal, L. Almasy, K. Bucholz, D.M. Dick, O. Harari, X. Xiaoling, V. Hesselbrock, J. Kramer, J.I. Nurnberger, J. Rice, M. Schuckit, J. Tischfield, B. Porjesz, H.J. Edenberg, L. Bierut, T. Foroud, A. Goate, Genome-wide survival analysis of age at onset of alcohol dependence in extended high-risk COGA families, Drug and Alcohol Dependence 142 (2014) 56-62.
[45] Z.B. Jiao, J.H. Luan, M.K. Miller, C.Y. Yu, C.T. Liu, Precipitate transformation from NiAl-type to Ni2AlMn-type and its influence on the mechanical properties of high-strength steels, Acta Materialia 110 (2016) 31-43.
[46] Y.S. Han, S.H. Hong, The effects of thermo-mechanical treatments on superplasticity of Fe-24Cr-7Ni-3Mo-0.14N duplex stainless steel, Scripta Materialia 36(5) (1997) 557-563.
[47] M. Pohl, O. Storz, T. Glogowski, Effect of intermetallic precipitations on the properties of duplex stainless steel, Materials Characterization 58(1) (2007) 65-71.
[48] Z.B. Jiao, J.H. Luan, M.K. Miller, Y.W. Chung, C.T. Liu, Co-precipitation of nanoscale particles in steels with ultra-high strength for a new era, (2017).
[49] J. Wan, H. Ruan, J. Wang, S. Shi, The Kinetic diagram of sigma phase and its precipitation hardening effect on 15Cr-2Ni duplex stainless steel, Materials Science & Engineering A 711(jan.10) (2017) 571-578.
[50] V.K. Vasudevan, S.J. Kim, C.M. Wayman, Precipitation reactions and strengthening behavior in 18 Wt Pct nickel maraging steels, Metallurgical Transactions A 21(10) (1990) 2655-2668.
[51] A.J. Ardell, Precipitation Hardening, Metallurgical and Materials Transactions A 16(12) (1985) 2131-2165.
[52] U.K. Viswanathan, G.K. Dey, V. Sethumadhavan, Effects of austenite reversion during overageing on the mechanical properties of 18 Ni (350) maraging steel, Materials Science and Engineering A 398(1-2) (2005) 367-372.
[53] C.J. McMahon, On the mechanisms of creep damage in type 316 stainless steel, Scripta Metallurgica 19(6) (1985) 733-737.

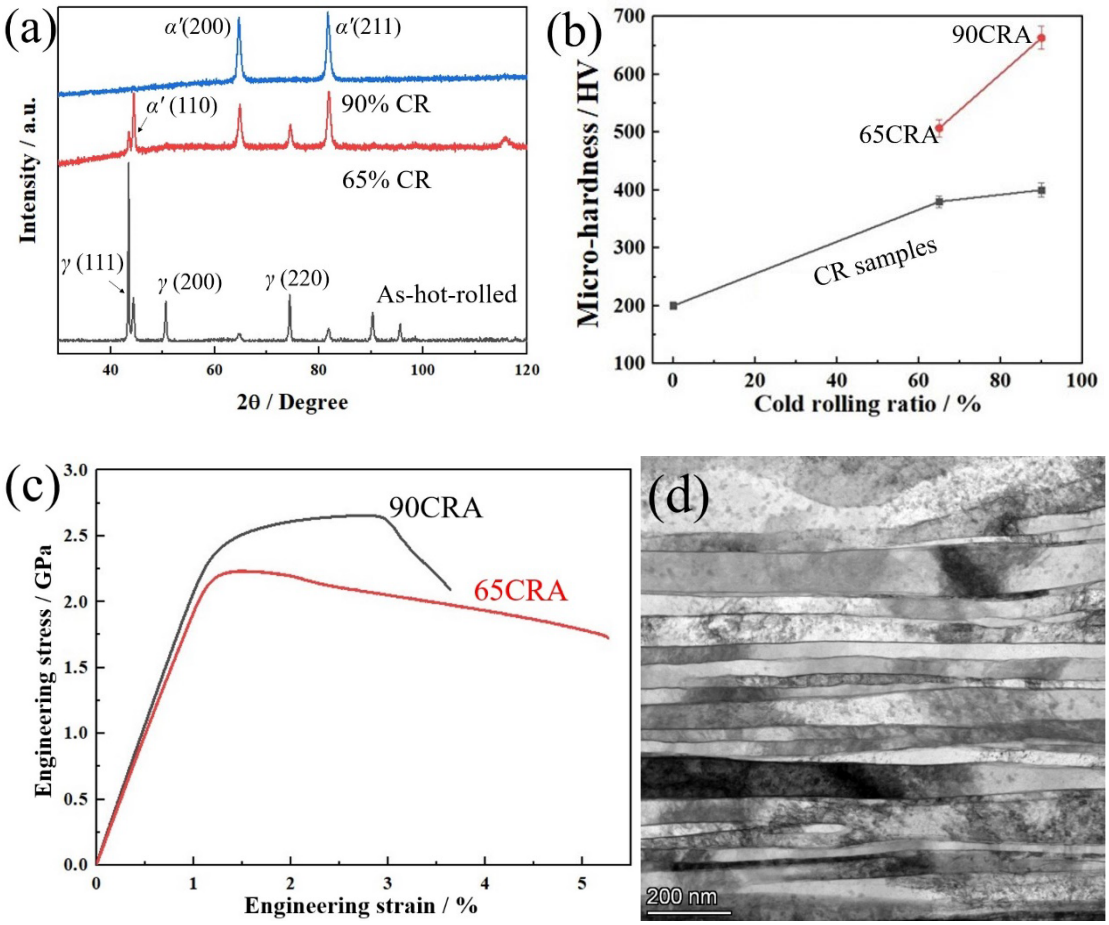

Fig. 1 (a) XRD patterns of the as-hot-rolled, 65% and 90% CR samples. (b) Vickers hardness of the as hot-rolled samples after different cold rolling ratios (black), 65CRA (red) and 90CRA (red). (c) Engineering stress-strain curves of the as-hot-rolled samples treated with 65%CR and 90%CR followed by ageing at 525 °C for 2 h, respectively (65CRA and 90CRA). (d) Bright-field TEM image of the 90CRA sample showing the elongated martensite laths.

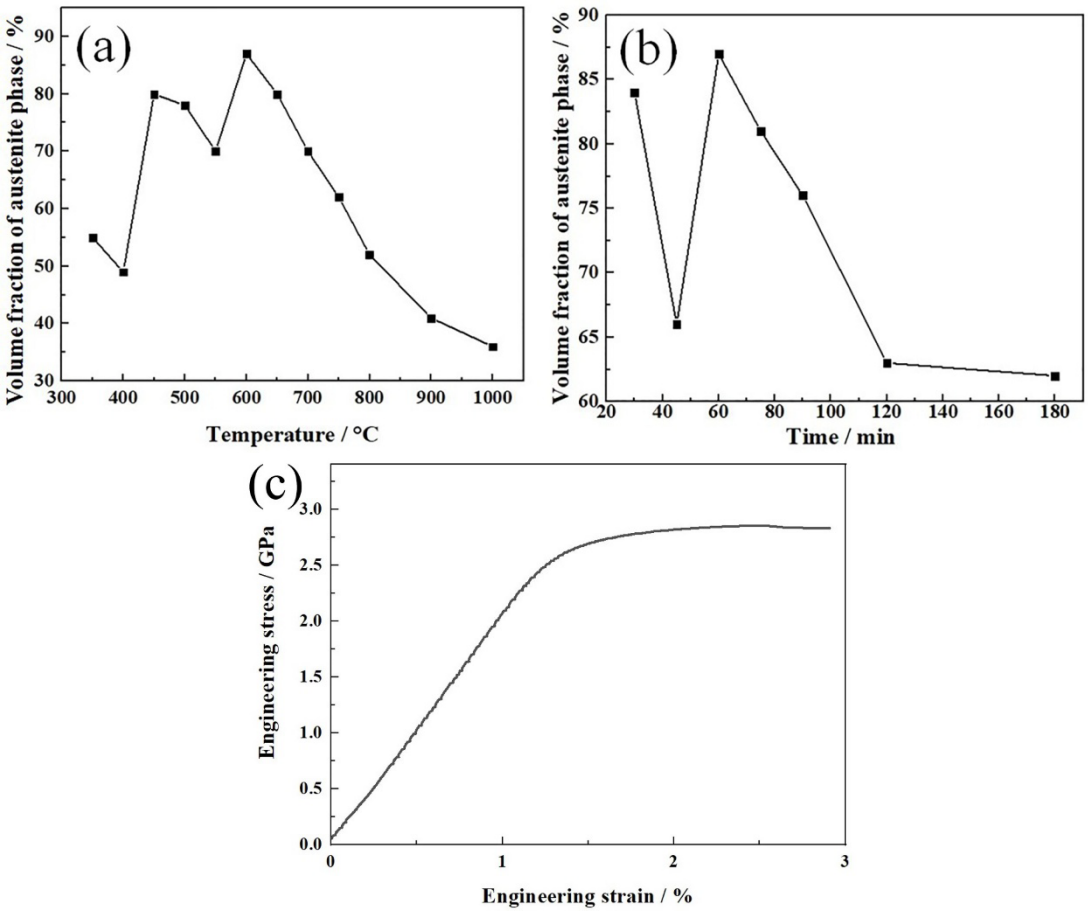

Fig. 2 Volume fractions of γ phase in the as-hot-rolled maraging steel depending on temperature for a fixed annealing time of 1 h (a) and annealing time at fixed 600 °C (b). (c) Engineering stress-strain curve of the as-hot-rolled sample solution-treated at 600 °C for 1 h followed with 90CR and then ageing at 525 °C for 2 h (600-90CRA).

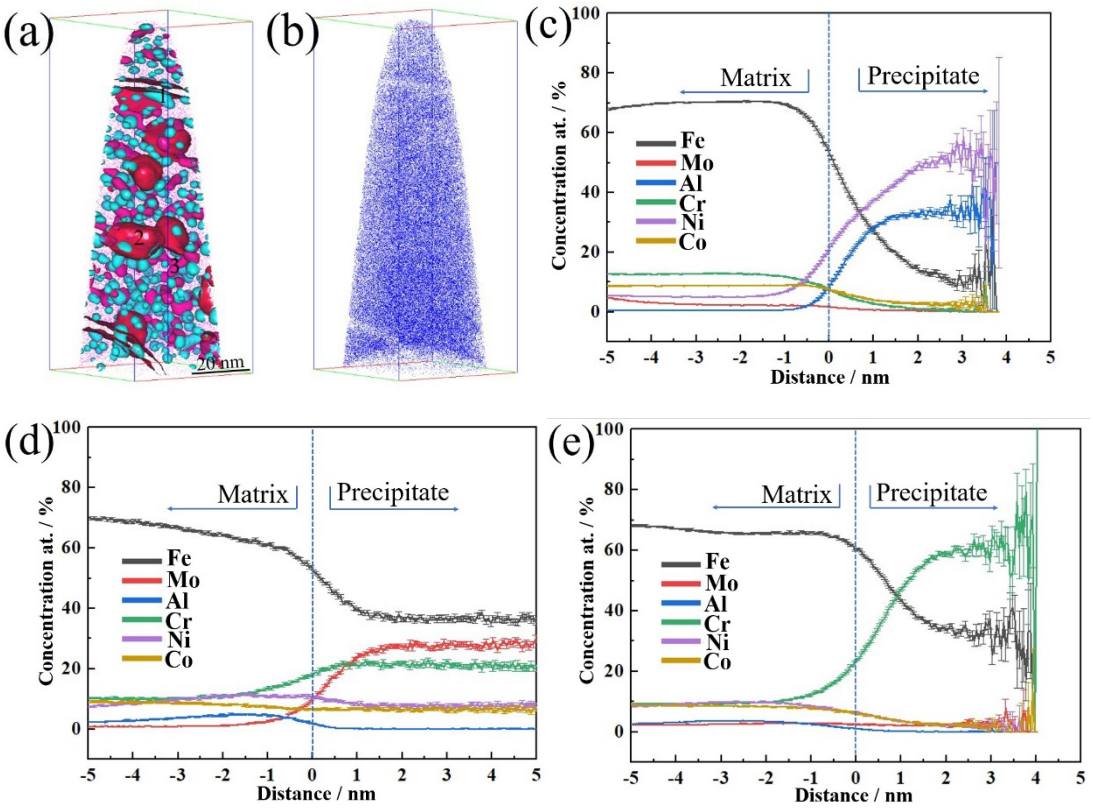

Fig. 3 Atom probe analysis showing tomography and composition of the precipitates in the 600-90CRA sample: (a) Iso-surfaces from APT of the steel, with Mo-enriched phase in yellow, NiAl in green and FeCr in purple; (b) Distribution profiles of Co atoms. Proximity histograms of the three precipitates 1, 2, and 3 in panel (a): (c) β-NiAl phase for 1, (d) Laves phase for 2 and (e) Sigma phase for 3.

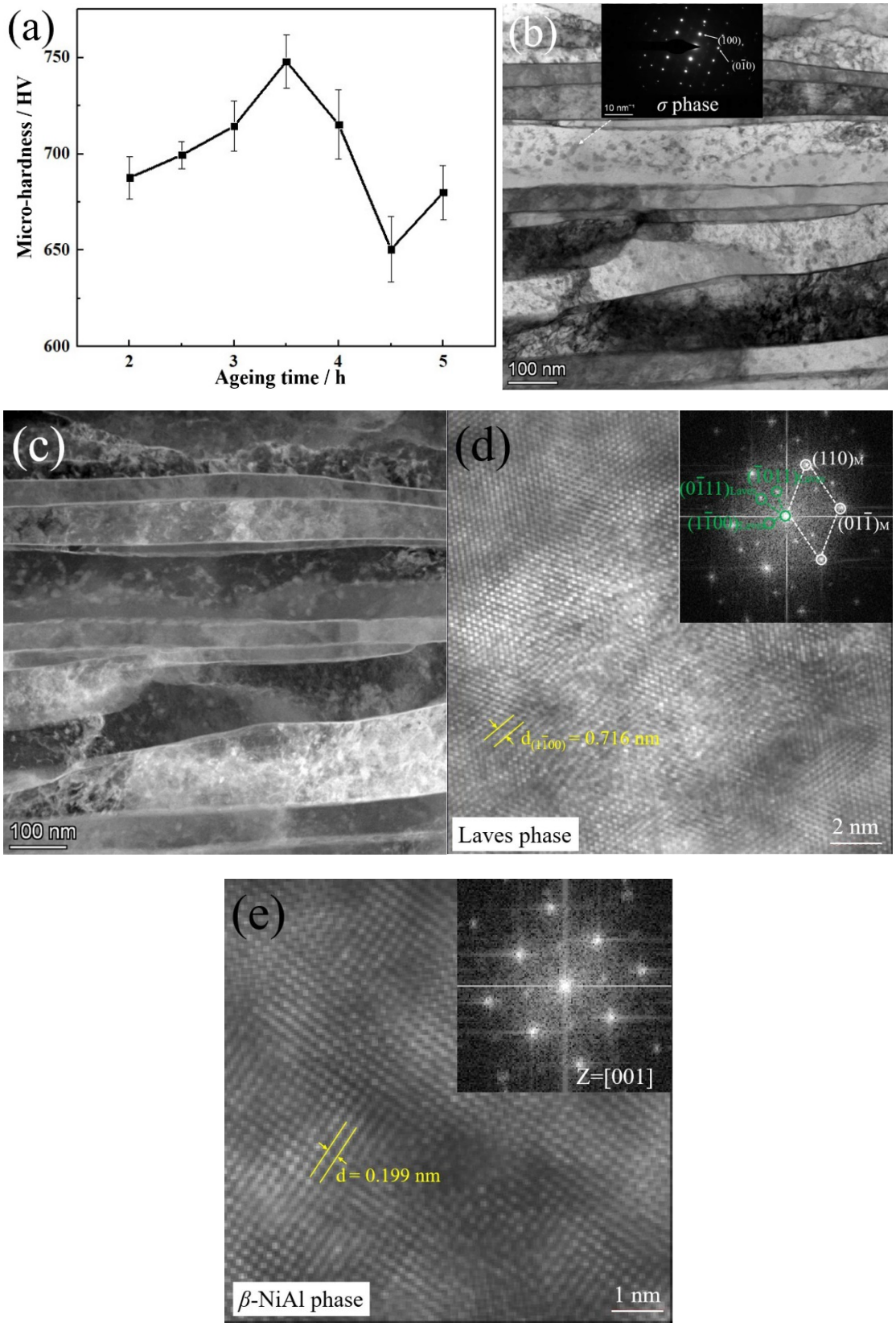

Fig. 4 (a) Micro-hardness of the as-hot-rolled steel samples solution-treated at 600 °C for 1 h followed with 90% CR and then ageing at 525 °C for 2 h (600-90CRA)~5 h,

respectively. (b) Bright field image of the 3.5h-aged sample before tensile test; (c) Dark field image of Fig. 4(b), showing precipitates and dislocations in the martensite laths. (d, e) HRTEM images corresponding to the Laves and β-NiAl phases, respectively, with the insets illustrating the FFT analysis results.

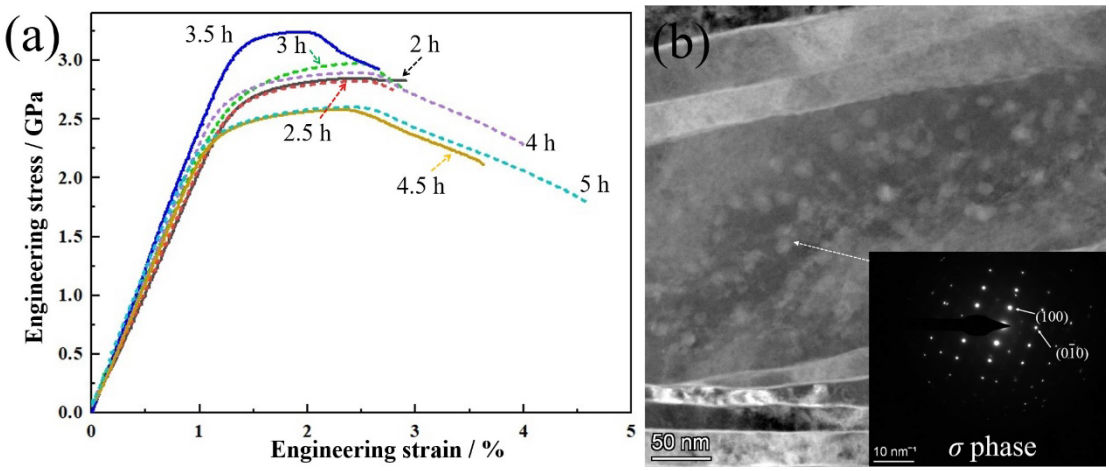

Fig.5 (a) Engineering stress-strain curves of the as-hot-rolled steel samples solution-treated at 600 °C for 1 h followed with 90% CR and then ageing at 525 °C for 2 h (600-90CRA)~5 h, respectively; (b) Dark field image of the 3.5h-aged sample after tensile test.